Microelectronic Engineering 108 (2013) 86–92

Contents lists available at SciVerse ScienceDirect

Microelectronic Engineering

journal homepage: www.elsevier.com/locate/mee

Field electron emission properties of vertically aligned carbon nanotubes deposited on a nanostructured porous silicon template: The hidden role of the hydrocarbon/catalyst ratio

N.A. Asli [a,b,*], M.S. Shamsudin [a,b,d], A.N. Falina [e], M.S. Azmina [e], A.B. Suriani [e], M. Rusop [a,c], S. Abdullah [a,b]

[a] Centre of Nanoscience and Nanotechnology (NANO-SciTech Centre), Institute of Science, Universiti Teknologi MARA, 40450 Shah Alam, Selangor D.E., Malaysia
[b] School of Physics and Material Studies, Faculty of Applied Sciences, Universiti Teknologi MARA, 40450 Shah Alam, Selangor D.E., Malaysia
[c] NANO-Electronic Centre, Faculty of Electrical Engineering, Universiti Teknologi MARA, 40450 Shah Alam, Selangor D.E., Malaysia
[d] University of Southampton Malaysia Campus (USMC), No. 3, Persiaran Canselor 1, Kota Ilmu Educity@Iskandar, 79200 Nusajaya, Johor D.T., Malaysia
[e] Department of Physics, Faculty of Science and Mathematics, Universiti Pendidikan Sultan Idris, 35900 Tanjung Malim, Perak D.R., Malaysia

ARTICLE INFO

Article history:
Available online 14 March 2013

Keywords:
Porous silicon
Carbon nanotubes
Catalyst ratio
Field emission
Botanical hydrocarbon

ABSTRACT

We report the observation of the field electron emission (FEE) of vertically aligned carbon nanotubes (VACNT) arrays grown on a nanostructured porous silicon template (NPSiT). VACNT were synthesised by a simple method using modified floated carbon source-catalyst in a two-stage hot filament thermal chemical vapour deposition system. Ferrocene was used as a catalyst in varying amounts from 0.3 to 0.8 g. An optimised NPSiT was used during the synthesis of VACNT. The surface morphology, lattice defects and graphitic structure of VACNT were analysed using a field emission scanning electron microscope and a high-resolution transmission electron microscope. The FEE performance of VACNT as synthesised is significantly affected by the hydrocarbon/catalyst ratio. The turn-on field required to extract a current density of 0.01 mA m^{-2} was 2.80 V μm^{-1}. The threshold field corresponding to a current density of 0.1 mA m^{-2} was 3.30 V μm^{-1}. The maximum current density of 1.2 mA m^{-2} was detected from a sample exhibiting optimum growth conditions. The emission stability and field enhancement factor β are also discussed in this paper.

1. Introduction

From theoretical and experimental studies, we know that carbon nanotubes (CNT) are an extraordinary material. CNT are commonly described as a sheet of graphene rolled into a seamless cylinder with a high aspect ratio. Since the landmark paper by Iijima that reported trials of a novel 1-dimensional (1-D) carbon nanostructure in the early 1990s [1], carbon nanotubes have attracted scientists, the business community and even the general public. Numerous studies have shown that CNT possess many extraordinary chemical, physical, electronic, and thermal properties [2–4]. Consequently, CNT have been proposed for use in many potential commercial applications including as electron field emitters [5,6], additives in lubricant [7,8], gas storage media [9,10] and many other fields. These applications have been pursued vigorously [11,12]. In next-generation display technology, CNT may be used as bright elements to produce perfect visual displays, such as high-definition flat panel displays, flexible-thin-paper displays and others.

A tremendous effort has been made to control the structure and characteristics of CNT by adjusting parameters such as their carbon precursors [13,14], the methods and apparatus used for their generation [15,16], the selection of a catalyst support [17,18], carbon and gas feeding rates [19,20] and other factors [21,22]. From the point of view of applications, a method to simply synthesise well-ordered arrays of VACNT is highly desirable. Chemical vapour deposition (CVD) methods (under certain conditions) are capable of producing better vertically aligned carbon nanotubes (VACNT) than other methods of nanotube production such as arc discharge and laser ablation [23]. It has been suggested that VACNT are easier to obtain when bottom growth occurs during the growth reaction, although VACNT can also be grown through a tip growth mechanism. VACNT consisting of very dense and closely packed CNT grow upwards, away from the substrate surface. This process is known as self-assembly or oriented growth [23]. In certain applications such as FEE, the synthesis of VACNT on a substrate is required. Growing VACNT with specified fine structure elements, including diameter, length, chirality and graphene layers, on a NPSiT is a challenging task. Fundamental questions remain regarding the

---

* Corresponding author at: Centre of Nanoscience and Nanotechnology (NANO-SciTech Centre), Institute of Science, Universiti Teknologi MARA, 40450 Shah Alam, Selangor D.E., Malaysia. Tel.: +60 172527436.

E-mail address: asnidasli@yahoo.com (N.A. Asli).

0167-9317/$ - see front matter © 2013 Elsevier B.V. All rights reserved.
http://dx.doi.org/10.1016/j.mee.2013.02.095

Table 1
Specification of Si wafer used in this experimental work.

Type of Si	*P*-type
Dopant	Boron
Resistivity (Ω cm)	1–10
Crystal orientation	⟨1 0 0⟩
Diameter (mm)	100
Thickness (μm)	525 ± 25

hydrocarbon/catalyst ratio process occurring during growth and its suitability for FEE applications.

Recently, several groups have reported the successful growth of VACNT on nanostructured templates. According to previous studies, CNT have the ability to emit cold electrons at relatively low voltages due to their controllable properties such as high aspect ratios, nanometer tip sizes [24], high density and well-ordered orientation [25]. Several groups have reported electron field emission from carbon nanotubes. The first reported field emission (FE) of electrons from isolated single multi-walled nanotubes (MWNT) wax by Rinzler et al. [26], who reported the FE when the nanotube tips were opened. This report was followed by Heer et al. [27], who reported FE from MWNT film. According to Saito et al. [28], CNT possess the following properties that make them favourable for FEE applications: (i) a high aspect ratio, (ii) sharp tips, (iii) high chemical stability and (iv) high mechanical strength. However, approximately 90% of the CNT literature still reports a μA cm^{-2} order of FE current density, and very few papers report CNT FE above 10 mA cm^{-2} operating in ultrahigh vacuum conditions [29–31]. In this paper, we studied vertically aligned carbon nanotubes grown on a nanostructured porous silicon template that emit an FE current density on the order of mA cm^{-2} with significant stability over a 3000 s duration.

We systematically investigate the hidden role of the hydrocarbon/catalyst ratio parameter on VACNT synthesis on an NPSiT. By tuning the hydrocarbon/catalyst ratio parameter, we have found optimised conditions for the growth of VACNT that offer better control of the following issues: (i) structural properties, (ii) undesired impurities, and (iii) uniformity and improved FEE performance. These findings enhance our understanding of the structural requirements of VACNT grown on a NPSiT and provide further information on the properties of FEE, including the potential to operate at low voltages, good emission stability and longer emitter lifetimes. We hope this article will provide guidance for future research.

2. Experimental methods and materials

2.1. Preparation of the nanostructured porous silicon template (NPSiT)

A detailed description of the preparation of a NPSiT is reported elsewhere [32,33], and the specifications of the Si wafers used is shown in Table 1. Before beginning our experiments, as a standard process, Si templates were prepared by cutting Si wafers to an area of 20 × 20 mm using a precision diamond cutter. The single-slide polished Si templates were ultrasonically cleaned in a mixture of acetone and methanol in a volume ratio of 1:1 for 5 min at 40 °C, and then thoroughly rinsed in de-ionised (DI) water several times. Si templates were kept at room temperature under controlled ambient (vacuum) overnight to avoid [34] (i) unwanted chemical impurities such as native oxides and (ii) moisture from the environment.

The experimental procedure for the formation of a NPSiT has been presented previously. In detail, the NPSiT was constructed through a custom-made photo-electrochemical anodisation setup, as shown in Fig. 1. The electrochemical-based solution (also known as an electrolyte solution) used in this approach was a mixture of ethanol and concentrated hydrofluoric acid (∼48%) with a volume fraction of 1:1. The photo-electrochemical anodisation setup is composed of a highly acidic resistant polymer such as Teflon, which is subsequently filled with a prepared electrochemical solution. To facilitate anodisation, (i) aluminium foil (serving as an anode) was sealed on the rear side of the Si template to form a good ohmic contact, and (ii) a tungsten electrode (serving as a cathode) was fixed at a 15 mm distance from the front surface of the Si template. An ‘o-ring’ was placed on the front side of the Si template to ensure that only the selected area was exposed to the electrolyte solution. The etching process was assisted by the illumination of a halogen lamp (120 W) and 20 mA/cm^2 of current density for 30 min. Finally, the NPSiT was rinsed in DI water and blown dry with nitrogen. As a result, the etched surface of the NPSiT appeared ‘yellowish’ and demonstrated visible light emission under UV light.

2.2. Synthesis of vertically aligned carbon nanotubes (VACNT) deposited on a NPSiT

VACNT deposited on a NPSiT were synthesised using a laboratory-scale method involving a two-stage hot filament thermal chemical vapour deposition (TCVD) system, as illustrated in Fig. 2. The experimental setup/configuration of this approach is described in previous experimental work [35–39]. The samples were prepared by varying the weight of ferrocene used (obtained from Sigma Aldrich) from 0.3 to 0.8 g, while maintaining the weight of camphor oil used at 5 g. The catalyst and the carbon source were placed in separate alumina boats and positioned side-by-side in furnace zone-1. The NPSiT was placed in the centre of furnace zone-2. Zone-2 was heated to 800 °C and was left to stabilise for 10 min, after which it was purged with nitrogen gas (0.05–1.00 L min^{-1}). Then, zone-1 was heated to 180 °C for the precursor vaporisation process. After zone-1 reached the required temperature, the synthesis process continued for 60 min. Nitrogen gas was continuously flowed before, during and after synthesis to prepare an ambient nitrogen environment. Zone-1 was turned off after the synthesis process was complete, and zone-2 was left on for 30 min after the annealing process. The samples were removed for characterisation after the furnaces cooled down to room temperature.

2.3. Characterisation process of VACNT deposited on a NPSiT

A field emission scanning electron microscope (FESEM; Carl Zeiss SMT 40VP) was employed to examine the morphological structure of VACNT. The graphitic and lattice structures of VACNT were examined by a high-resolution transmission electron microscope (HRTEM; JEOL JEM 2100F). To obtain optimal FEE characteristics, FEE measurements were performed in a parallel-plate electrode configuration with stainless steel electrodes (10 × 10 mm sample area), with a cathode-to-anode separation distance of 0.25 mm and in a vacuum environment of 10^{-4} Torr working pressure.

3. Results and discussion

Fig. 4 shows typical field emission scanning electron microscopy (FESEM) top-view images for low and high magnifications of carbon nanotubes with varying amounts of catalyst. The low-magnification images show uniform growth and vertical alignment as the amount of ferrocene increases. The relationship between the growth rate of VACNT and the amount of ferrocene (Fe) used (from 0.3 to 0.8 g with 5 g camphor oil) is shown in Fig. 3. The growth

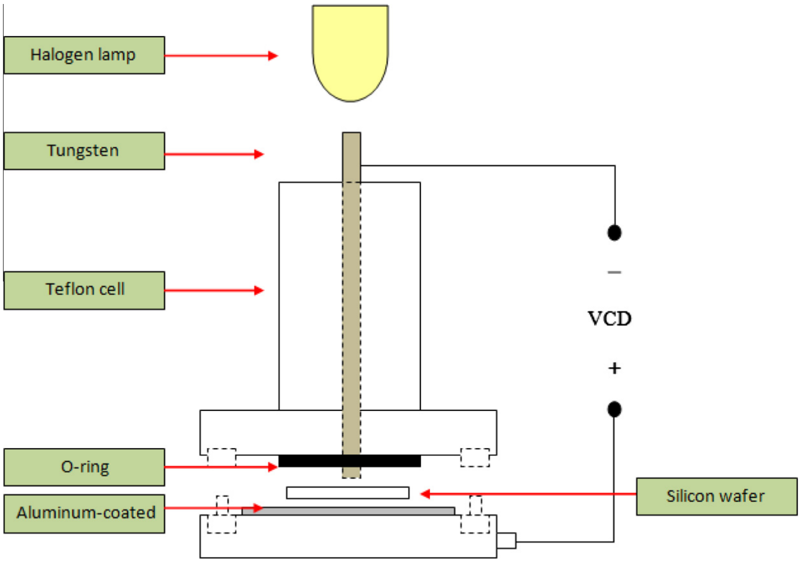

Fig. 1. Drawing of the custom-made of photo-electrochemical anodization apparatus. A: halogen lamp; B: electrochemical solution; C: cathode; D: anode; E: silicon template; o-ring; G: Teflon cell; H: retort stand.

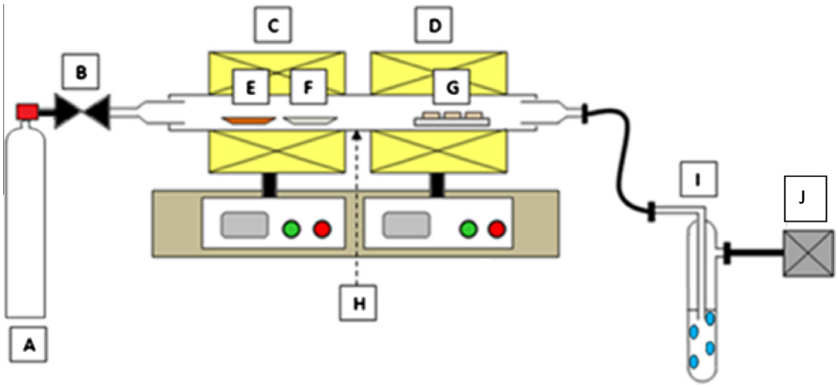

Fig. 2. The schematic diagram of VACNT formation production set-up used. A: nitrogen gas tank; B: gas controller; C: first furnace; D: second furnace; E: camphor oil; F: ferrocene; G: NPSiT; H: furnace separator; I: bubbler; J: exhaust.

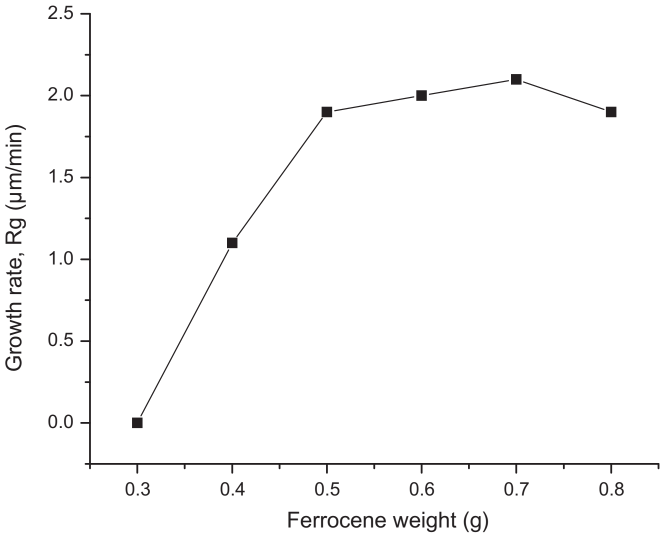

Fig. 3. The VACNT growth rate at different ferrocene ratio.

rate can be calculated as $\alpha = \beta\,(\mu m)/\gamma\,(min)$ [40], where β is the distribution length of the tubes and γ is the deposition time. As the amount of ferrocene increases from 0.3 to 0.4 g, the growth rate of the VACNT increases rapidly from 0 to 1.9 $\mu m\ min^{-1}$. The growth rate continues to increase gradually, with a maximum rate of 2.1 $\mu m\ min^{-1}$ found for a sample catalysed with 0.7 g of ferrocene. The growth rate decreases to 1.9 $\mu m\ min^{-1}$ with 0.8 g of ferrocene. Fig. 4a shows the shorter lengths and poor vertical alignment of nanotubes as a result of the small amount of Fe particles needed to catalyse the growth of VACNT. The reduced growth rate of the sample synthesised at 0.8 g ferrocene was a result of the low catalytic activity resulting from the incremented Fe particle sizes. Fig. 4f shows VACNT that contain impurities, which result in a larger nanotube diameter. These impurities may be the result of the large amount of ferrocene that decomposes to an abundance of Fe particles, which tend to agglomerate in large clusters.

The density of CNT grown on a NPSiT can be observed in the low-magnification images in Fig. 4a–f. Fig. 4c shows a sample grown with a high VACNT density and uniform nanotubes. As mentioned before, the density of CNT plays a crucial role in the FEE properties of nanotubes. The structure of CNT also significantly affects their FEE properties. Fig. 5 shows a high-resolution transmission electron microscopy (HRTEM) image of specimens grown with

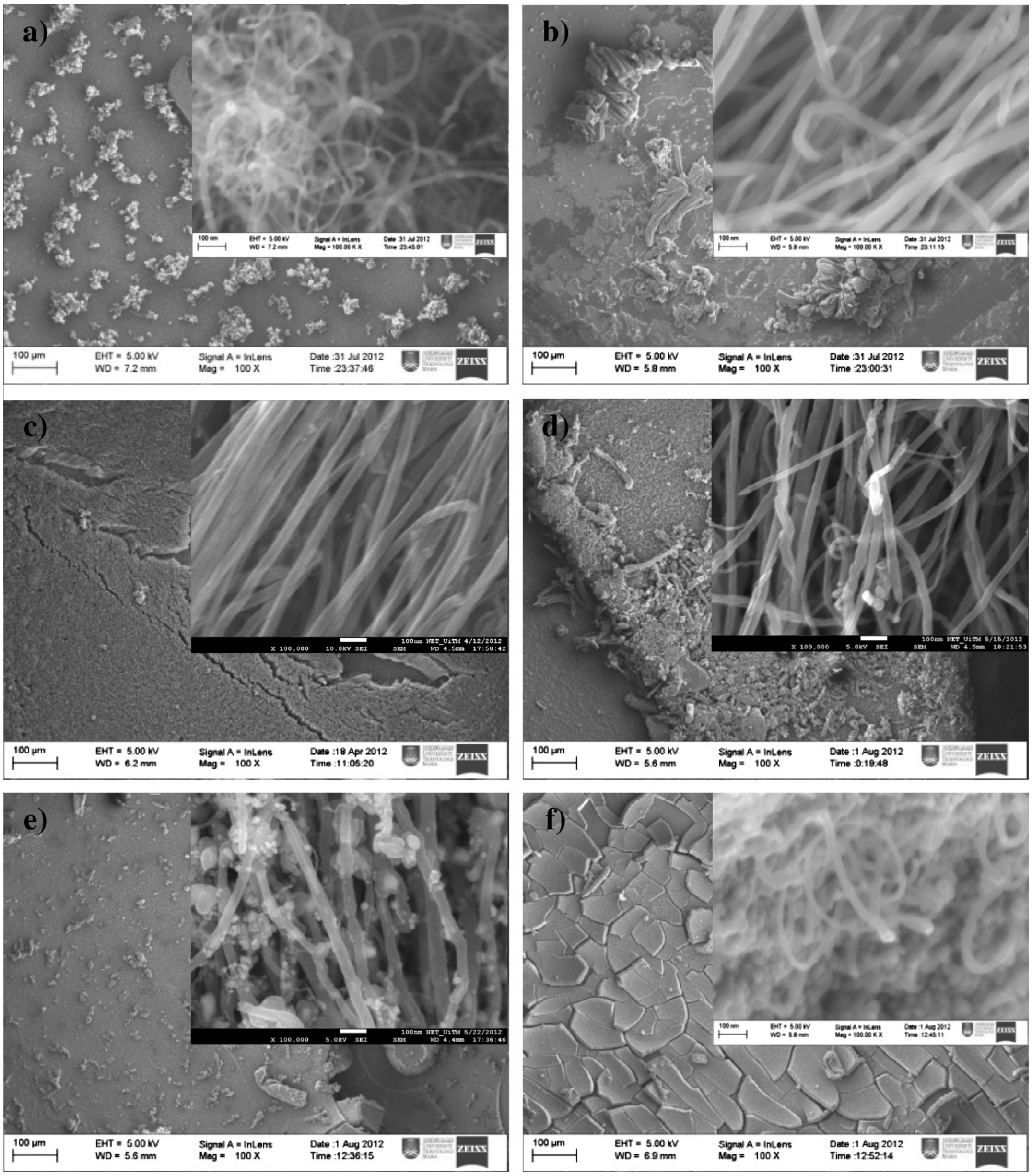

Fig. 4. FESEM micrographs of VACNT at different Fe ratio: (a) 0.3 g, (b) 0.4 g, (c) 0.5 g, (d) 0.6 g, (e) 0.7 g, (f) 0.8 g.

different amounts of ferrocene, which reveal CNT structures with multi-walled, hollow and bamboo-like block structures. Specimens grown with 0.5 g ferrocene have many blocks compared to other specimens, a condition that is believed to improve the field emission of VACNT.

Fig. 6a presents J–E curves obtained from CNT synthesised with different amounts of ferrocene (0.3–0.8 g) and 5 g of camphor oil. Here, the turn-on field and threshold field are defined as the fields required to extract a current density of 0.01 and 0.1 mA cm^{-2}, respectively. The field emission properties associated with all the tested ferrocene amounts are compared in Table 2. The turn-on values were found to decrease from 3.20 V µm^{-1} to a minimum value of 2.80 V µm^{-1} as the amount of ferrocene increased from 0.3 to 0.5 g for a 5 g precursor. As the amount of ferrocene increased to 0.8 g, the turn-on value increased to 3.06 V µm^{-1}. The threshold field was also found to decrease to a minimum value of 3.30 V µm^{-1} for 0.5 g ferrocene. The maximum current density (J_{max}) was found to be 1.2 mA cm^{-2} at a field of 4.40 V µm^{-1}, which was shown by sample synthesis using 0.5 g ferrocene for 5 g of camphor oil. J_{max} increased as the amount of ferrocene increased to its maximum value, and thereafter decreased sharply. Therefore, we believed that a controlled increase of ferrocene might help strengthen the current density [41]. These data are comparable to and are even better than earlier published FEE reports [42,43].

The field enhancement factor β was calculated from a Fowler–Nordheim (F–N) plot corresponding to the J–E curves. The β value can be derived with the Fowler–Nordheim formula, which is discussed in detail by Li et al. [43]. According to the F–N relation, $J = A\beta^2E^2/\exp(-B^{3/2}/\beta E)$ with $A = 1.54 \times 10^{-6}$ AV^{-2} eV, the emission current density of a nanotube tip is dependent on the local field, E_{loc}, and the work function φ of the emitter tip. It is believed that the current emission of CNT occurs from multiple emitters, and an average current was measured [44]. E_{loc} was related to the macroscopic electric field (the external field applied), E, which was amplified at the emitter tip by factor β; therefore, the effective local field is $E_{loc} = \beta E$.

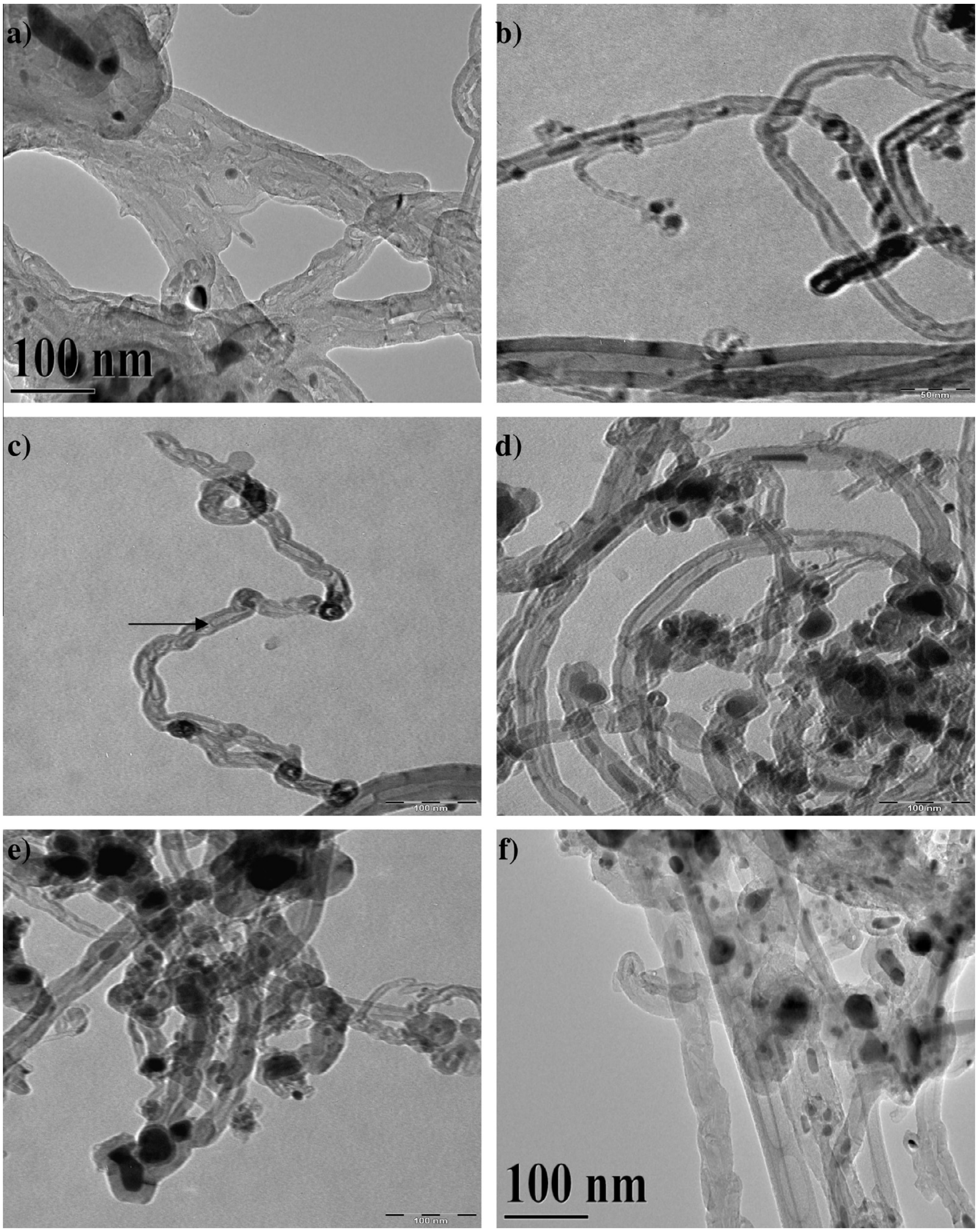

Fig. 5. HRTEM image showing a detailed of multiwalled and bamboo-like structure of carbon nanotubes field emitters at different Fe ratio: (a) 0.3 g, (b) 0.4 g, (c) 0.5 g, (d) 0.6 g, (e) 0.7 g, (f) 0.8 g.

A linear *F–N* curve was obtained by plotting $\ln J/E^2$ as a function of $1/E$, indicating that the current was generated by field emitted electrons [42]. The experimental *F–N* plots obtained for all ferrocene ratios are shown in Fig. 6b. Table 1 shows β values as calculated from the equation $\beta = -B\varphi^{3/2}$/slope of *F–N* curve, where the CNT φ value was ~5 eV [45] and $B = 6.83 \times 109\ \mathrm{eV}^{-3/2}\ \mathrm{Vm}^{-1}$. The calculated β for ferrocene amounts from 0.3 to 0.8 g were found in the range 1235.9–1572.9. These ranges are acceptable for field emission devices where the literature reports β value for CNT prepared by chemical vapour deposition technique of 200–2000 in aligned CNT deposits [46]. Of the tested ferrocene amounts, 0.5 g resulted in the highest calculated β. This result shows that the E_{loc} was strongly applied in the CNT catalysed at this ratio as compared with other samples [47]. We confirmed that the low turn-on and threshold field values and the increase in the maximum emission current density observed in this sample were caused by enhanced local electric fields due to the enhanced β on the nanotube tips.

Emission current stability tests were performed out on the same sample. The current stability of VACNT on NPSiT synthesised with various ferrocene amounts (0.3–0.5 g) with 5 g of camphor oil are presented in Fig. 7. The display current of 0.01 mA as a function of time with a 3000 s duration was plotted at various applied voltages. As shown in Fig. 7a, for a sample catalysed by 0.3 g of ferrocene, obvious current emission degradation together with spikes and slight fluctuations in emission were detected. For a sample catalysed by 0.4 g of ferrocene (shown in Fig. 7b), the emission dropped significantly after 250 s from approximately 0.40 to 0.28 mA. The current emission degraded continuously to 0.20 mA after 3000 s. These results indicate insufficient quality for flat panel display technology.

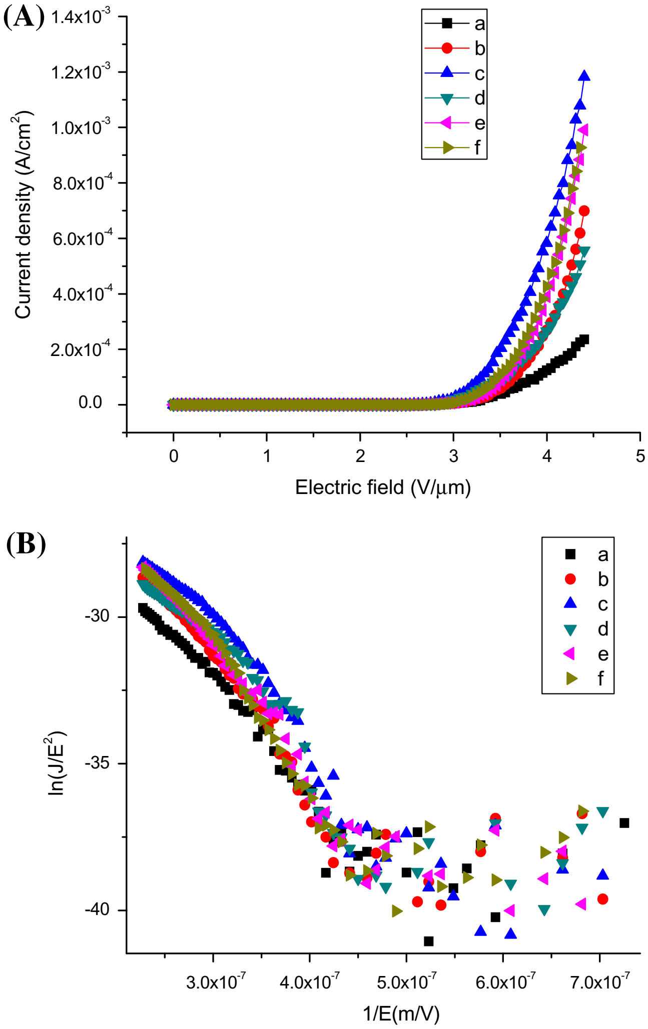

Fig. 6. (A) Third cycle of J–E curves of VACNT as a function of ferrocene ratio, (B) Corresponding F–N plots as a function of ferrocene ratio: (a) 0.3 g, (b) 0.4 g, (c) 0.5 g, (d) 0.6, (e) 0.7 g, (f) 0.8 g.

Table 2
FEE characteristic of VACNT as a function of ferrocene ratio (0.3–0.8 g).

Camphor oil: ferrocene ratio (g)	Turn on field (V µm^{-1}) at 0.01 mA cm^{-2}	Threshold field (V µm^{-1}) at 0.1 mA cm^{-2}	J_{max} (mA/cm^2)	β Values
5:0.3	3.20	3.90	0.24	1235.9
5:0.4	3.09	3.65	0.70	1653.0
5:0.5	2.80	3.30	1.20	1758.8
5:0.6	2.94	3.60	0.56	1740.0
5:0.7	3.05	3.54	0.99	1653.1
5:0.8	3.06	3.47	0.92	1572.9

As the amount of ferrocene used increased to 0.5 g (Fig. 7c), the emission loss gradually improved. The current sharply dropped from approximately 0.98 to 0.70 mA after 250 s and was then stabilised until 3000 s. For samples catalysed at 0.6, 0.7 and 0.8 g ferrocene (Fig. 7d–f), emission loss and several current spikes were detected approximately 250 s. These results reveal that an increase in the amount of ferrocene used aids the stability and improves the lifetime of field emission display effectively. Samples prepared with 0.5 g ferrocene exhibited more stable current emission, less degradation, fewer spikes and a lower signal to noise ratio.

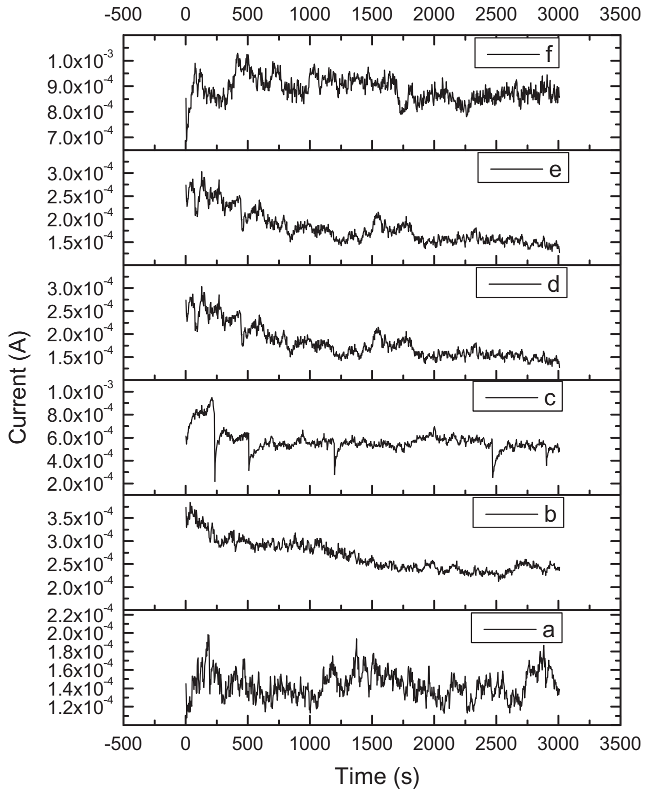

Fig. 7. Current stability measurement done on CNT for 50 min as a function of ferrocene ratio: (a) 0.3 g, (b) 0.4 g, (c) 0.5 g, (d) 0.6, (e) 0.7 g, (f) 0.8.

4. Conclusion

We have reported a simple method for growing vertically aligned multi-walled carbon nanotubes by modified two-stage catalytic-nanotemplate thermal chemical vapour deposition. We attribute the differences in the field emission properties observed to the amount of ferrocene used as a catalyst. All CNT samples catalysed from 0.3 to 0.8 g of ferrocene exhibited turn-on fields of less than 4 V µm^{-1} and their emission currents approach 1.2 mA cm^{-2} for a field of 4.5 V µm^{-1}. Moreover, our well-aligned nanotubes have stable emissions and are strong candidates for electron emitter applications.

Acknowledgements

This work was financially supported by the Malaysian Ministry of Higher Education through the Fundamental Grant Research Scheme under contact no. 600-RMI/ST/FRGS 5/3/Fst 204/2010 and Universiti Teknologi MARA through the Young Lecturer Scheme and Excellence Fund under contact no. 600-RMI/ST/DANA 5/3/Dst 20/2011. We are thankful to the anonymous reviewers who kindly give us valuable feedback to improve this manuscript. Thanks are also due to Prof. Roslan Md Nor from the University of Malaya for very useful discussions on FEE theory.

References

[1] Sumio Iijima, Nature 354 (1991) 56–58.
[2] Jan-Hendrik Pöhls, Michel B. Johnson, Mary Anne White, Rachit Malik, Brad Ruff, Chaminda Jayasinghe, Mark J. Schulz, Vesselin Shanov, Carbon 50 (2012) 4175–4183.
[3] Gilbert D. Nessim, Nanoscale 2 (2010) 1306–1323.
[4] Rodney S. Ruoff, Donald C. Lorents, Carbon 33 (1995) 925–930.
[5] Indranil Lahiri, Wonbong Choi, Acta Mater. 59 (2011) 5411–5421.

[6] J.L. Kwo, Meiso Yokoyama, W.C. Wang, F.Y. Chuang, I.N. Lin, Diamond Relat. Mater. 9 (2000) 1270–1274.

[7] C.S. Chen, X.H. Chen, L.S. Xu, Z. Yang, W.H. Li, Carbon 43 (2005) 1660–1666.

[8] C.S. Chen, X.H. Chen, J. Hu, H. Zhang, W.H. Li, L.S. Xu, Z. Yang, Trans. Nonferrous Met. Soc. China 15 (2005) 300–305.

[9] C.W. Tan, K.H. Tan, Y.T. Ong, A.R. Mohamed, S.H.S. Zein, S.H. Tan, Environ. Chem. Lett. 10 (2012) 265–273.

[10] K.L. Lim, H. Kazemian, Z. Yaakob, W.R.W. Daud, Chem. Eng. Technol. 33 (2010) 213–226.

[11] S.M. Sanip, A.F. Ismail, P.S. Goh, T. Soga, M. Tanemura, H. Yasuhiko, Sep. Purif. Technol. 78 (2011) 208–213.

[12] N. Timizar, Info Chim. Mag. 43 (2006) 6–11.

[13] Jianguo Zhao, Xiangyun Guo, Quangui Guo, Ling Gu, Yong Guo, Feng Feng, Carbon 49 (2011) 2155–2158.

[14] I. Suarez-Martinez, N.A. Marks, Carbon 50 (2012) 5441–5449.

[15] S. Santangelo, M. Lanza, E. Piperopoulos, S. Galvagno, C. Milone, Mater. Res. Bull. 47 (2012) 595–601.

[16] A. Gohier, T.M. Minea, S. Point, J.-Y. Mevellec, J. Jimenez, M.A. Djouadi, A. Granier, Diamond Relat. Mater. 18 (2009) 61–65.

[17] M.Z. Hussein, S.A. Zakarya, S.H. Sarijo, Z. Zainal, J. Nanomater. 2012 (2012). Article ID 525616, 9 pages.

[18] Placidus B. Amama, Cary L. Pint, Francesca Mirri, Matteo Pasquali, Robert H. Hauge, Benji Maruyama, Carbon 50 (2012) 2396–2406.

[19] QiXin Liu, YuLu.Yin.Zhang. Ouyang, Lu Yin Zhang, Yan Xu, Yan Fang, Physica E 41 (2009) 1204–1209.

[20] S. Porro, S. Musso, M. Giorcelli, A. Chiodoni, A. Tagliaferro, Physica E 37 (2007) 16–20.

[21] Illayathambi Kunadian, Rodney Andrews, M. Pinar Mengüç, Dali Qian, Chem. Eng. Sci. 64 (2008) 1503–1510.

[22] Illayathambi Kunadian, Rodney Andrews, Dali Qian, M. Pinar Mengüç, Carbon 47 (2009) 384–395.

[23] K.B.K. Teo, C. Singh, M. Chhowalla, W.L. Milne, Catalytic Synthesis of Carbon Nanotubes and Nanofibers, in Encyclopedia of Nanoscience and Nanotechology, vol. X, American Scientific Publisher, 2003. pp. 1–22.

[24] Jung Inn Sohn, Y.-H. Sohn, S.-Y. Choi, K.-I. Cho, K.-S. Nam, Appl. Phys. Lett. 78 (2001) 901–903.

[25] J. Li, W. Lei, X. Zhang, B. Wang, L. Ba, Solid-State Electron. 48 (2004) 2147–2151.

[26] A.G. Rinzler, J.H. Hafner, P. Nikolaev, L. Lou, S.G. Kim, D. Tomanek, P. Nordlander, D.T. Colbert, R.E. Smalley, Science 269 (1995) 1550–1553.

[27] W.A.D. Heer, A. Châtelain, D. Ugarte, Science 270 (1995) 1179–1180.

[28] Y. Saito, S. Uemura, Carbon 38 (2000) 169–182.

[29] S. Fan, M.G. Chapline, N.R. Franklin, T.W. Tombler, A.M. Cassel, H. Dai, Science 283 (1999) 512–514.

[30] L. Gangloff, E. Minoux, K.B.K. Teo, P. Vincent, V.T. Semet, V.T. Binh, M.H. Yang, I.Y.Y. Bu, R.G. Lacerda, G. Pirio, J.P. Schnell, D. Pribat, D.G. Hasko, G.A.J. maratunga, W.I. Milne, P. Legagneux, Nano Lett. 4 (2004) 1575–1579.

[31] S.H. Jo, D.Z. Wang, J.Y. Huang, W.Z. Li, K. Kempa, Z.F. Ren, Appl. Phys. Lett. 85 (2004) 810–812.

[32] N.A. Asli, S.F.M. Yusop, M. Rusop, S. Abdullah, Ionics 17 (2011) 653–657.

[33] S.F.M. Yusop, M. Rusop, S. Abdullah, Mater. Res. Innovations 15 (2011) 210–212.

[34] M. Grunder, H. Jacob, Appl. Phys. A 39 (1986) 73–82.

[35] M.S. Shamsudin, A.B. Suriani, S. Abdullah, S.Y.S. Yahya, M. Rusop, J. Spectrosc. 2013 (2013). Article ID 167357.

[36] M.S. Shamsudin, M.F. Achoi, M.N. Asiah, L.N. Ismail, A.B. Suriani, S. Abdullah, S.Y.S. Yahya, M. Rusop, J. Nanomater. 2012 (2012) Article ID 972126, 5 pages.

[37] M.S. Shamsudin, M. Maryam, N.A. Asli, S.A.M. Zobir, M.A. Johari, S.F.M. Yusop, A.B. Suriani, S. Abdullah, S.Y.S. Yahya, M. Rusop, Nano Hybrids 2 (2012) 25–42.

[38] M. S. Shamsudin, N. A. Asli, S. Abdullah, S. Y. S. Yahya, M. Rusop, Adv. Condens. Matter. Phys. 2012 (2012) Article ID 420619, 7 pages.

[39] M.S. Shamsudin, I.A. Lahori, A.B. Suriani, S. Abdullah, S.Y.S. Yahya, M. Rusop, Adv. Mater. Res. 576 (2012) 454–458.

[40] A.B. Suriani, A.A. Azira, S.F. Nik, R. Md Nor, M. Rusop, Mater. Lett. 63 (2009) 2704–2706.

[41] Mukul Kumar, Tsugio Okazaki, Mineo Hiramatsu, Y. Ando, Carbon 45 (2007) 1899–1904.

[42] S.P. Somani, P.R. Somani, M. Tanemura, S.P. Lau, M. Umeno, Curr. Appl. Phys. 9 (2009) 144–150.

[43] W.L.J. Li, X. Zhang, B. Wang, L. Ba, Solid-State Electron. 48 (2004) 2147–2151.

[44] S.K. Srivastava, V.D. Vankar, D.V. Sridhar Rao, V. Kumar, Thin Solid Films 515 (2006) 1851–1856.

[45] M. Kumar, K. Kakamu, T. Okazaki, Y. Ando, Chem. Phys. Lett. 385 (2004) 161–165.

[46] M. Sveningsson, R.E. Morajan, O.A. Nerushev, Y. Sato, J. Backstrom, E.E.B. Campbell, F. Rohmund, Appl. Phys. A 73 (2001) 409–418.

[47] J.H. Choi, S.H. Choi, J.H. Han, J.B. Yoo, C.Y. Park, J. Appl. Phys. 94 (2003) 487–490.